A temporal assessment of fully polarimetric multifrequency SAR observations over the Canadian permafrost

Paloma Saporta[a,b], Alberto Alonso-González[a], Irena Hajnsek[a,b]
[a] Microwaves and Radar Institute, German Aerospace Center, Germany
[b] Institute of Environmental Engineering, ETH Zürich, Switzerland

Abstract

In the frame of the PermASAR campaign, DLR's F-SAR instrument collected valuable multifrequency fully-polarimetric acquisitions in summer 2018 and winter 2019 over several permafrost regions in Canada. The present study proposes a first polarimetric analysis over Trail Valley Creek – one of the test sites characterized by continuous permafrost. We examine the influence of frequency, season and vegetation diversity on the scattering mechanisms occurring at the ground surface.

1 Introduction

In the Northern hemisphere, rising air temperatures lead to an increase of permafrost thawing, with many environmental implications. The increase of active layer depth modifies energy, carbon and water cycles at local and global scale. Permafrost thaw also induces ground settling which jeopardizes settlement, infrastructures and industrial activities. Finally, permafrost thaw can occasionally release bacteria, viruses, wastes and chemicals in the atmosphere and through runoff of water, these materials can pose risks for Arctic wildlife and human health.

Permafrost monitoring benefits from the spatial coverage enabled by remote sensing techniques as compared to the sparsity of pointwise measurements, as permafrost regions cover a substantial part of the Northern hemisphere land (about a quarter of the terrestrial surface). The penetration capabilities of airborne radar signals into the ground could be exploited to investigate subsurface processes and properties, on which the future permafrost degradation depends. In this paper we assess the influence of frequency, season and vegetation diversity on the scattering mechanisms occurring at the ground surface using airborne Synthetic Aperture Radar data of DLR over a selected test site in Northern Canada.

2 Data description

2.1 The PermASAR campaign

The PermASAR campaign [1] consisted in two successive missions: the first one in summer 2018 and the second one in early spring 2019, in order to record signals from both thawed and frozen permafrost ground. The campaign aimed at investigating the interaction between radar signals at different wavelengths and permafrost soils. More specifically, parameters relative to the permafrost thermal state (soil moisture, active layer thickness), in relation with the vegetation cover, are of interest. For this purpose, the F-SAR, DLR's state-of-the art airborne SAR instrument, was operated in fully polarimetric mode at several bands (X,C,S,L) over several test sites in Canada. Nine test sites

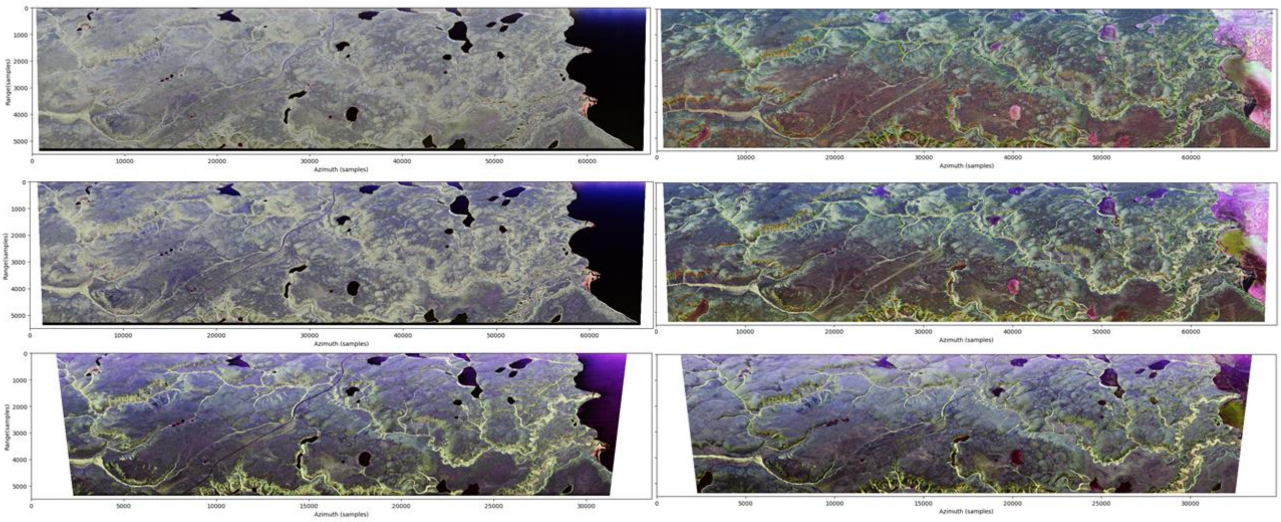

Figure 1 Pauli RGB representation of the fully polarimetric acquisitions in summer 2018 (left column) and winter 2019 (right column). Red, green and blue stand for powers in HH-VV, HV+VH and HH+VV respectively. From top to bottom, rows correspond to X-, C- and L-band data.

https://ieeexplore.ieee.org/document/9944279

extending over 2000 km in the North-South direction have been chosen. The imaged regions are characterized by different types of terrains, with landscapes ranging from forest over discontinuous permafrost (taiga) to continuous permafrost covered by shrubs (tundra).
In this study, we focus on one particular test site which covers the Trail Valley Creek catchment - an extensively monitored area due to the presence of the Trail Valley Creek Research Station. In order to assess the variability of the scattering responses with frequency, fully polarimetric data were acquired over the site with wavelengths of 3 cm, 6 cm and 23 cm. (i.e. at X-, C- and L-band). The corresponding Pauli images are shown on **Figure 1**. Investigations are performed jointly with the Alfred Wegener Institute (AWI) in the frame of the "Hidden Image of Thawing Permafrost "project. [2]

2.2 Acquisitions over Trail Valley Creek test site

The Trail Valley Creek catchment is located within the North West Canadian Arctic tundra and is characterized by ice-rich continuous permafrost, resulting in seasonal changes of the ground thermal state. In summer, the ground consists in a thawed layer of soil above frozen soil. The active layer thickness is at largest of 25 to 100 cm [3]. In winter, the ground is frozen and covered by a heterogeneous snow layer. At Trail Valley Creek, the permafrost reaches 100 to 150 m thickness. [3].
The two acquisitions analysed here were carried out on the 15th of August 2018 and on the 23rd of March 2019 respectively, that is, during permafrost stable phases i.e. outside of the active thaw and freeze phases. The SAR images cover about 14 x 5 km and extend over several landcover types: tree patches, shrubs, tussock, lichen, lakes. We selected several patches according to their vegetation cover during the polarimetric analysis; they are shown on **Figure 2**. The vegetation is only partially covered by snow in winter.

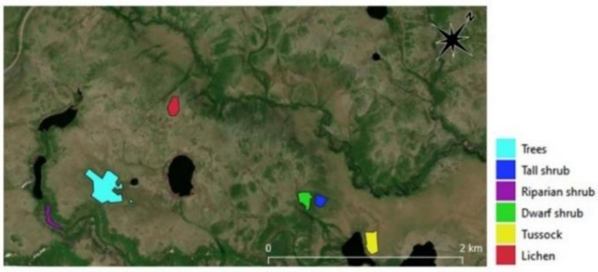

Figure 2 Patches of homogeneous vegetation type used for the analysis**,** underlain by software QGIS optical basemap of ESRI.

3 Method

In order to characterize the scattering occurring on the ground by means of the fully polarimetric dataset, we perform an entropy/ α angle decomposition as described in [4]. The parameters entropy H and mean α angle represent respectively the randomness of the scattering process occurring on the ground, and the mean type of scattering mechanism. The decomposition is applied on both summer and winter scenes, and for each wavelength. We further isolate patches with homogeneous landcover following the classification issued by [5], and extract the H/α parameters over each patch. The different vegetation types are: lichen (3-5 cm height), tussock (10-30 cm height), dwarf shrub (20-50 cm height), riparian shrub (up to 2.1 m tall), tall shrub (up to 2 m tall), trees (up to 10 m tall).

We further perform a polarimetric change analysis following the method defined in [6]. This approach allows the characterization of the type and the amount of change between two fully polarimetric SAR images by determining the polarization states that maximize (respectively minimize) the contrast between the two images. Starting from two coherency matrices associated with one acquisition each, the range of values spanned by a certain polarimetric contrast measure is extracted from the generalized eigendecomposition between those two matrices, defined as the problem $T_2 w = \lambda T_1 w$. The generalized eigenvalues $\lambda_1, \lambda_2, \lambda_3$ correspond to the maximum, intermediate and minimum polarimetric contrast, and the eigenvectors w_1, w_2, w_3 correspond to the polarization states associated with the eigenvalues. Eigenvalues larger (respectively smaller) than 1 indicate an increase (respectively decrease) in backscattered power. To represent the information in a concise way, two indicators are defined that sum up the increasing (respectively decreasing) contributions by weighting the polarization states by the amount of change they represent:

$$\mathbf{p}_{inc} = 10\left[\sum_{i\,|\,\lambda_i>1} (log(\lambda_i)\mathbf{p}_i)^2\right]^{\frac{1}{2}}$$

and

$$\mathbf{p}_{dec} = 10\left[\sum_{i\,|\,\lambda_i<1} (-log(\lambda_i)\mathbf{p}_i)^2\right]^{\frac{1}{2}}$$

p_{inc} and p_{dec} thus contain information on the amount of change (intensity) and the type of change (color).

Finally, we consider more specifically copolar phase differences (CPD) defined here as $\Phi_c = \Phi_{HH} - \Phi_{VV}$, in relation to the snow cover. A phase difference between two concomitant HH and VV images is occasioned by the differential propagations of the electro-magnetic waves at different polarisations within the snowpack. Copolar phase differences at X-band have been related to snow structure, snow depth and acquisition geometry for instance in [7].

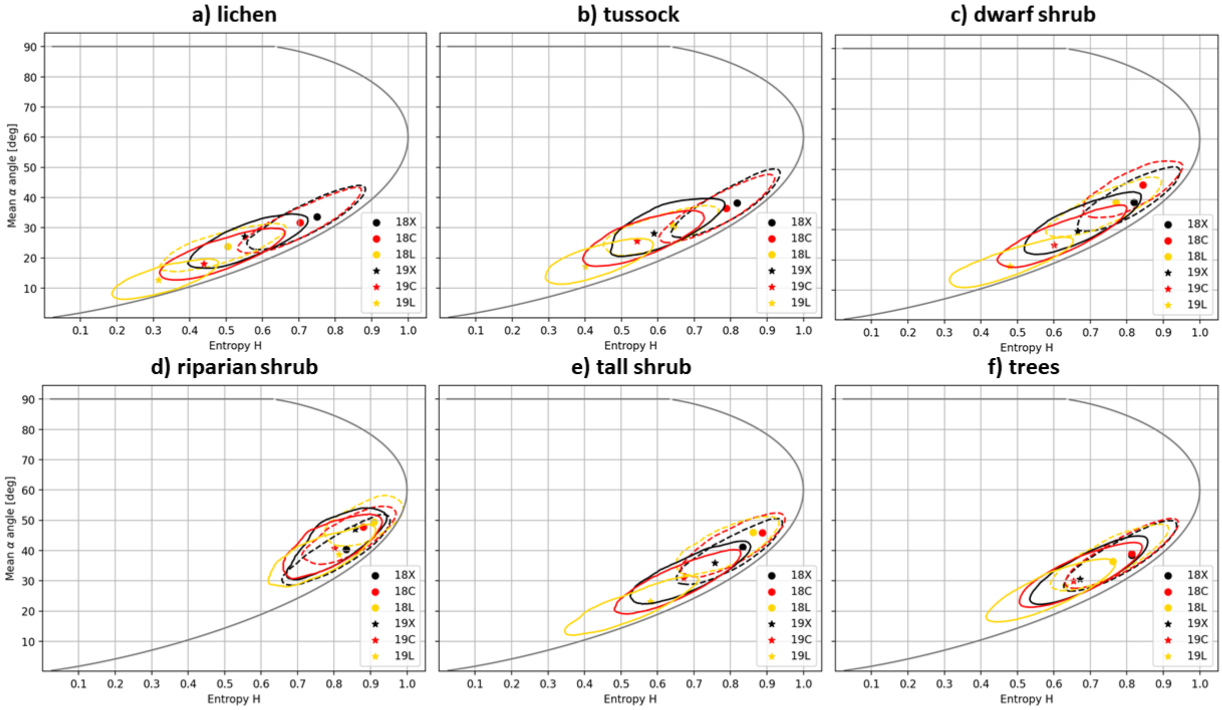

Figure 3 Normalized two-dimensional H/α histograms for several vegetation types. Lines represent contour plots at a fixed density threshold, taken at 0,1 in order to account for the overall distribution. Dashed and solid lines stand respectively for summer and winter data. Circles and stars indicate the location of the density maximum. Vegetation types are ordered (from left to right) by increasing vegetation height: lichen, tussock, dwarf shrub, riparian shrub, tall shrub, trees. The solid gray line delineates the achievable H and α values.

The snow depth map used for this analysis has been deduced from the DEM of the sow-covered landscape in April 2018, taking as reference a DEM of the bare ground, as issued in [5].

4 Results and discussion

4.1 H/ α analysis

A preliminary analysis of H and α over the whole imaged region yields the following observations:

- In summer: H and α show little variation between X- and C- band. At L-band, H and α values are overall smaller than at X- and C-band. For fixed wavelength and season, larger H and α values are observed at areas with slopes and areas with significant vegetation.
- Inter-band relations are the same in winter than in summer, but H and α are overall shifted towards lower values.

Let us now consider the influence of vegetation type. The outcome of the H/α decomposition on particular patches characterized by their vegetation type is shown on **Figure 3**. Overall, the values observed are typical for Bragg surfaces, rough surfaces and vegetation.

All 36 H/α histograms are computed for a given frequency (X-, C-, L-band), season (winter/summer) and vegetation type. In the following section the analysis and a first order interpretation are done on the different observables.

First, we observe that the patch of riparian shrub tundra exhibits a singular behaviour compared to all other vegetation types. The pixels of this class barely show any diversity in frequency or season, except a slight increase of H and α with wavelength in summer. We exclude it from the following observations.

Frequency diversity

In winter, there is a rather large diversity between all 3 bands for most vegetation types, in particular for smaller vegetation (lichen, tussock, dwarf shrub). Trees however only show small frequency diversity between X- and C-band.

In summer, tall shrubs and trees histograms barely show any frequency dependency. Smaller vegetation types (lichen, tussock, dwarf shrub) do not demonstrate some diversity between X- and C- band either, however H and α values at L-band are significantly smaller than at smaller wavelengths.

Seasonal diversity

At L-band, all vegetation types show large differences between winter and summer; it is particularly the case for dwarf shrub tundra and tall shrub tundra.

At X- and C-band, all vegetation types show some differences between summer and winter. Globally, the seasonal diversity is larger at C-band than X-band.

Winter frozen soils tend to be characterized by surface-like scattering (trend towards lower H/α) while summer thawed soils tend to be dominated by volume-like scattering (the

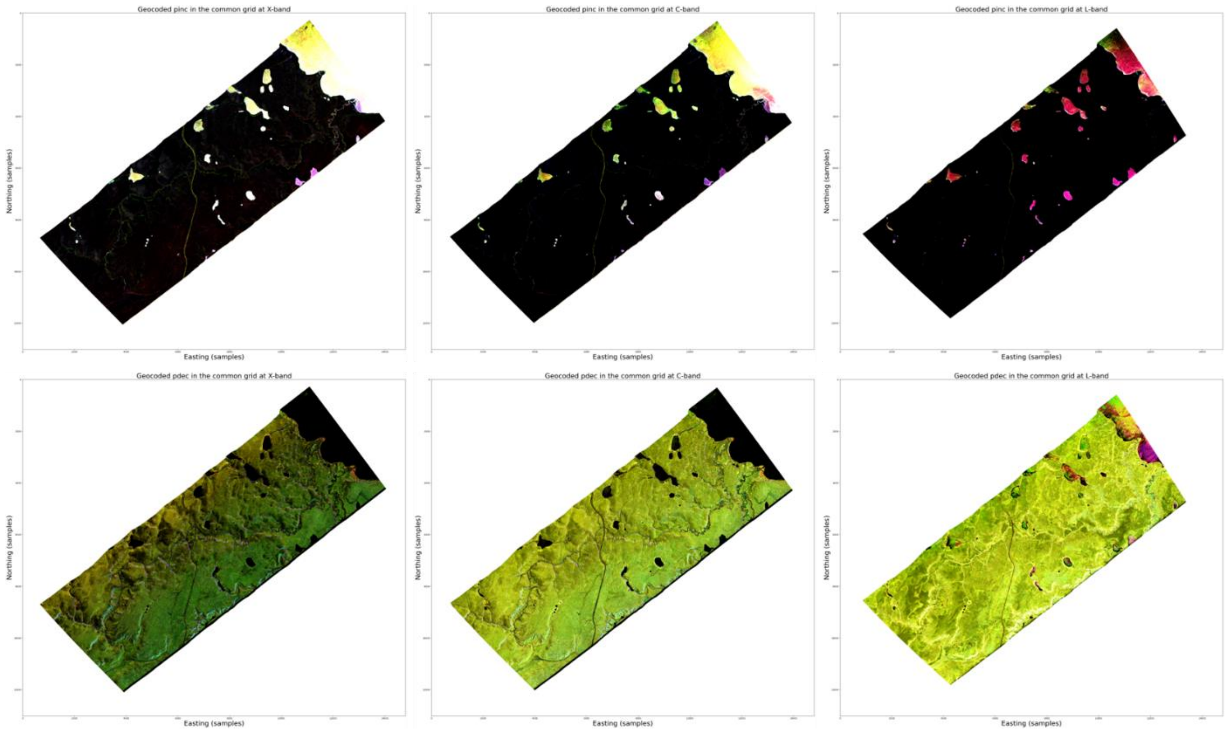

Figure 4 Polarimetric change representation of the differences from summer 2018 to winter 2019 in the Pauli basis (red: HH-VV, green: HV, blue: HH+VV). Each channel is scaled from 1 to 10 dB.

trend is going towards larger H/α). This observation agrees with the conclusions of previous studies performed at C-band [8][9][10].

Vegetation diversity

The differences in vegetation type introduce the most visible diversity at L-band; at X-band on the contrary, H/α histograms barely vary with vegetation. Overall, a trend in increasing both H and α for increasing vegetation height appears.

It should be noted that the pixels classified as trees here encompass lower vegetation as the trees are rather sparsely distributed in the chosen patch. Furthermore, snow could be a factor impacting the estimation in winter.

4.2 Polarimetric change

4.2.1 Temporal change at fixed bands

The polarimetric change between summer and winter is represented on **Figure 4** with the indicators p_{inc} and p_{dec}. We observe first a clear difference between water bodies and ground areas. Water bodies, which surface is frozen in winter and non-frozen in summer, show a general increase (winter w.r.t summer) in all bands, predominantly in the HH-VV channel at X- and L-band, and in the HV channel at C-band.

Over the ground areas, there is a general decrease in scattering power in winter with respect to summer, and the decrease is scaling with the considered band: the change increases in magnitude as the wavelength increases. For all wavelengths, the changes occur predominantly in the HV

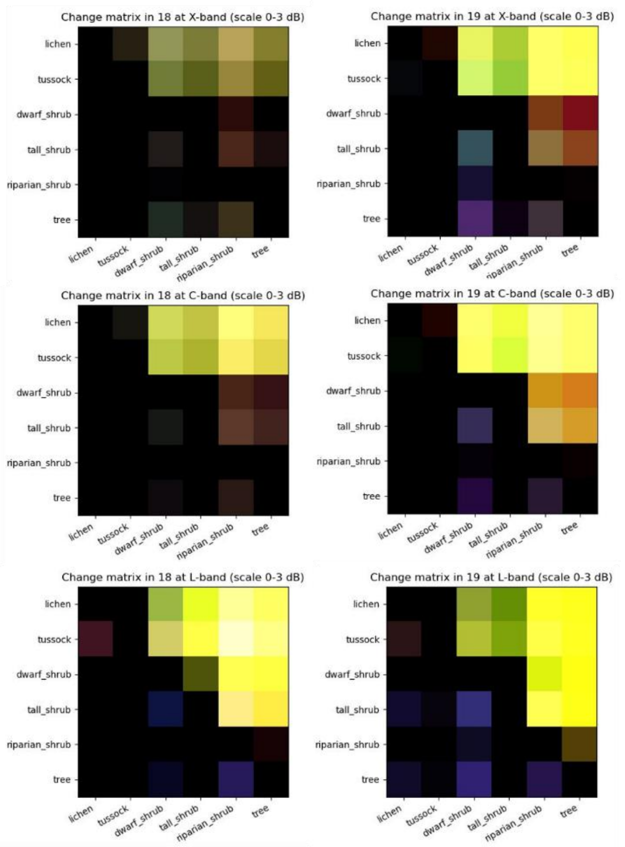

Figure 5 Change matrices summarizing the polarimetric change between vegetation types for different seasons and bands. The upper diagonal contains p_{inc} values, the lower diagonal p_{dec} values in the Pauli basis, scaled between 0 and 3 dB. The diagonal is set to 0 dB (black).

channel, secondarily in the HH-VV channel, and compared to those the change associated with the HH+VV polarisation is negligible. These results are consistent with the previous observation in 4.1 that there is a shift from volume-like scattering in summer to more surface-like scattering in winter.
There are several possible sources of the change in the scene. The presence of snow in winter, compared to its absence in summer, potentially introduces a change in polarimetric type and power. The frozen state of the soil and of the vegetation in winter, per opposition to their non-frozen state, could also introduce changes. The magnitude of these effects is expected to be function of the considered wavelength.

4.2.2 Landcover change

The change analysis is performed at landcover level to compare different vegetation types with another. As a single pixel is associated to a single landcover, the change analysis of [6] is performed using the coherency matrices averaged over all the pixels of a given landcover class. Vegetation classes are ordered as follows: lichen, tussock, dwarf shrub, tall shrub, riparian shrub, tree, corresponding to an increasing vegetation height. The change analysis is performed on land covers with higher vegetations with respect to land covers with smaller vegetation. Results are summed up in a change matrix representing the power of the change in between all combinations of vegetation types, for each band and each season separately (**Figure 5**). Globally, there is an increase in polarimetric scattering power from smaller to higher vegetation. Change occurs predominantly in the HV and HH-VV channels (green and red). Some pairs of similar landcovers (lichen vs tussock, tall shrub vs dwarf shrub, riparian shrub vs tree) show very little to no change. This is coherent with the 2x2 blocks in the upper matrix. Globally, intensities of change are larger while moving away from the diagonal, that is, the change is larger as the difference in vegetation height increases.

4.3 CPD in relation to snow depth

The spatial variations of the CPD at X-band in winter show similar patterns than the snow depth distribution, as shown on **Figure 6**: areas with significant (positive or negative) CPD correspond to areas with large snow depth. The histogram on **Figure 6** indicates that there is a certain trend over the entire area covered by the snow map of increasing CPD for increasing snow depth. It can be noted that one expects CPD to contain both contributions from propagation effects such as the differential propagation into snow, and scattering effect linked for instance to the geometry of the ground. Summer snow-free CPD however encompasses only the scattering effects, and these effects are small in magnitude (**Figure 6 c**) when compared to winter (**Figure 6 d**). This is an indication that the large CPD in winter could be due to snow [7].

5 Outlook

Future work should include soil moisture estimation using a model-based approach to separate volume scattering from surface scattering and further applying a soil moisture model on the surface scattering component. The decomposition can be performed either with the presented eigenvalue decomposition or with a model-based approach such as the Freemann-Durden decomposition, like presented in [8]. A third approach is to use polarimetric SAR interferometry in order to separate volume from ground contribution and to invert soil moisture from the latter, as in [11].

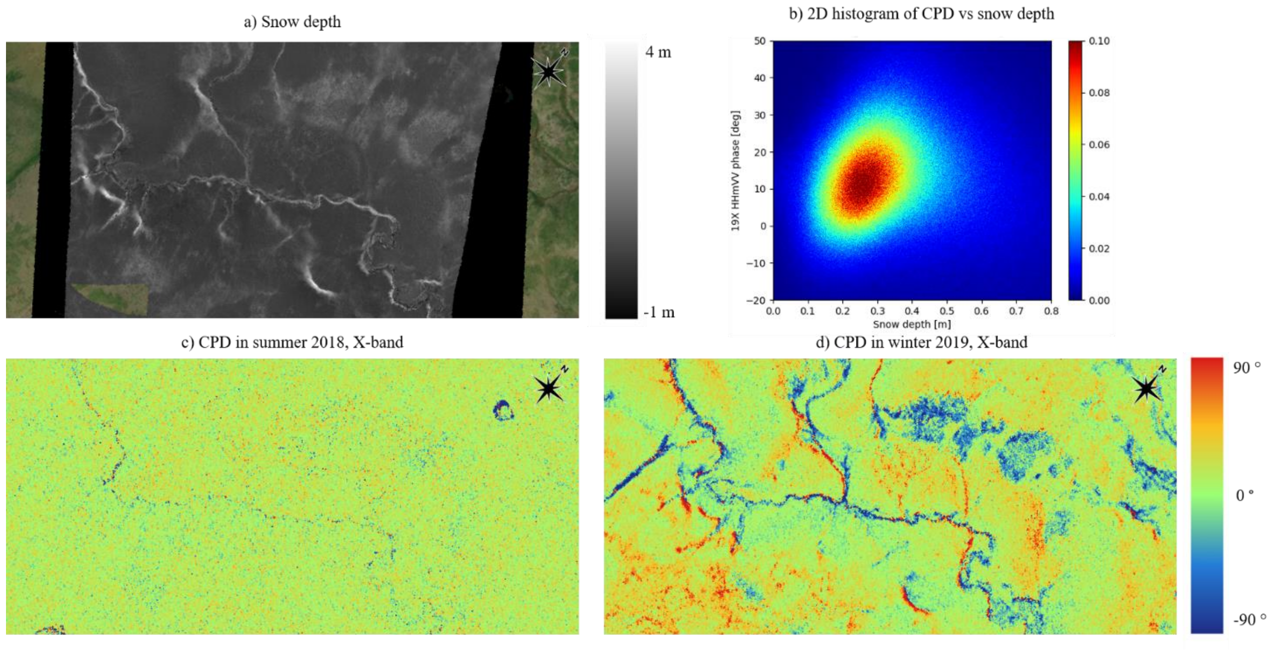

Figure 6 Focus on one subset of the area for which snow depth data is available, and the corresponding CPD maps in summer 2018 and winter 2019, at X-band. The histogram is computed for all pixels covered by the snow depth map.

6 Acknowledgements

We would like to thank Julia Boike and Inge Grünberg (Alfred Wegener Institute) for sharing their maps of vegetation map and snow over the test area.

7 Literature

[1] I. Hajnsek, H. Joerg, R. Horn, M. Keller, D. Gesswein, M. Jaeger, R. Scheiber, P. Bernhard, S. Zwieback, "DLR Airborne SAR Campaign on Permafrost Soils and Boreal Forests in the Canadian Northwest Territories, Yukon and Saskatchewan: PermASAR", POLINSAR 2019; 9th International Workshop on Science and Applications of SAR Polarimetry and Polarimetric Interferometry, 2019.

[2] I. Grünberg, "The Hidden Image of Thawing Permafrost: Mapping Subsurface Properties and Taliks with Remote Sensing", Helmholtz Imaging Virtual Conference 2021, 23 September 2021.

[3] I. Grünberg, E.J. Wilcox, S. Zwieback, P. Marsh, and J. Boike, "Linking tundra vegetation, snow, soil temperature, and permafrost", Biogeosciences, 17(16), 4261-4279, 2020.

[4] J.S. Lee and E. Pottier, "Polarimetric radar imaging: from basics to applications", CRC press, 2017.

[5] I. Grünberg and J. Boike, "Vegetation map of Trail Valley Creek, Northwest Territories, Canada", PANGAEA, https://doi.org/10.1594/PANGAEA.904270, 2019.

[6] A. Alonso-González, C. López Martínez, K. Papathanassiou, and I. Hajnsek, I, "Polarimetric SAR time series change analysis over agricultural areas". IEEE transactions on geoscience and remote sensing, 58(10), 7317-7330, 2020

[7] S. Leinss, G. Parrella and I. Hajnsek, „Snow height determination by polarimetric phase differences in X-band SAR data". IEEE Journal of Selected Topics in Applied Earth Observations and Remote Sensing, 7(9), 3794-3810, 2014

[8] T. Jagdhuber, J. Stockamp, I. Hajnsek and R. Ludwig, "Identification of soil freezing and thawing states using SAR polarimetry at C-band", Remote Sensing, 6(3), pp. 2008–2023, 2014.

[9] J. Khaldoune, E. van Bochove, M. Bernier, and M.C. Nolin, "An approach for mapping frozen soil of agricultural land under snow cover using RADARSAT-1 and RADARSAT-2", In IGARSS 2008-2008 IEEE International Geoscience and Remote Sensing Symposium, vol. 3, pp. III-382, 2008

[10] L.P Rousseau, R. Magagi, R. Leconte, A. Berg and B. Toth, "Potentials of RADARSAT-2 data to monitor freezing/thawing cycles over agricultural lands in Canada", In 2009 IEEE International Geoscience and Remote Sensing Symposium, vol. 2, pp. II-598, 2009.

[11] A. Alonso-Gonzalez and K. P. Papathanassiou, "Polarimetric Change Analysis in Forest using PolInSAR Ground and Volume separation techniques," EUSAR 2021; 13th European Conference on Synthetic Aperture Radar, pp. 1-6, 2021